Status and motivation of Raman LIDARs development for the CTA Observatory

M. DORO[1,2,3], M. GAUG[2,3], J. PALLOTTA[4], G. VASILEIADIS[5], O. BLANCH[6], F. CHOUZA[4], R. D'ELIA[4], A. ETCHEGOYEN[7], LL. FONT[2,3], D. GARRIDO[2,3], F. GONZALES[4], A. LÓPEZ-ORAMAS[6], M. MARTÍNEZ[6], L. OTERO[4], E. QUEL[4], P. RISTORI[4], FOR THE CTA CONSORTIUM

[1] *Univ. and INFN Padova, via Marzolo 8, 35131 Padova (Italy),* [2] *Física de les Radiacions, Departament de Física, Universitat Autònoma de Barcelona, 08193 Bellaterra, Spain,* [3] *CERES, Universitat Autònoma de Barcelona-IEEC, 08193 Bellaterra, Spain,* [4] *CEILAP (CITEDEF-CONICET), UMI-IFAECI-CNRS (3351) - Buenos Aires, Argentina,* [5] *LUPM. Montepellier, France,* [6] *IFAE, 08193 Bellaterra, Spain,* [7] *ITeDA (CNEA CONICET - UNSAM) - Buenos Aires, Argentina.*

michele.doro@pd.infn.it

Abstract: The Cherenkov Telescope Array (CTA) is the next generation of Imaging Atmospheric Cherenkov Telescopes. It would reach unprecedented sensitivity and energy resolution in very-high-energy gamma-ray astronomy. In order to reach these goals, the systematic uncertainties derived from the varying atmospheric conditions shall be reduced to the minimum. Different instruments may help to account for these uncertainties. Several groups in the CTA consortium are currently building Raman LIDARs to be installed at the CTA sites. Raman LIDARs are devices composed of a powerful laser that shoots into the atmosphere, a collector that gathers the backscattered light from molecules and aerosols, a photosensor, an optical module that spectrally select wavelengths of interest, and a read-out system. Raman LIDARs can reduce the systematic uncertainties in the reconstruction of the gamma-ray energies down to 5% level.

All Raman LIDARs subject of this work, have design features that make them different than typical Raman LIDARs used in atmospheric science, and are characterized by large collecting mirrors ($\sim$ 2 m^2). They have multiple elastic and Raman read-out channels (at least 4) and custom-made optics design. In this paper, the motivation for Raman LIDARs, the design and the status of advance of these technologies are described.

Keywords: monitoring, calibration, LIDAR, aerosols, gamma rays, cosmic rays, CTA

1 Introduction

Currently in its design stage, the Cherenkov Telescope Array (CTA) is an advanced facility for ground-based very-high-energy gamma-ray astronomy [1]. It is an international initiative to build the next-generation Cherenkov telescope array covering the energy range from a few tens of GeV to a few hundreds of TeV with an unprecedented sensitivity. The design of CTA is based on currently available technologies and builds upon the success of the present generation of ground-based Cherenkov telescope arrays (H.E.S.S., MAGIC and VERITAS [1]).

Nowadays, the main contribution to the systematic uncertainties of imaging Cherenkov telescopes stems from the uncertainty in the height- and wavelength-dependent atmospheric transmission for a given run of data. Atmospheric quality affects the measured Cherenkov yield in several ways: the air-shower development itself, the loss of photons due to scattering and absorption of Cherenkov light out of the camera field-of-view, resulting in dimmer images and the scattering of photons into the camera, resulting in blurred images. Despite the fact that several supplementary instruments are currently used to measure the atmospheric transparency, their data are only used to retain good-quality observation time slots, and only a minor effort has been made to routinely correct data with atmospheric information [4, 5, 6]. This situation may change with the CTA atmospheric monitoring and calibration program [20]. There are several goals behind this program. The first is to increase the precision and accuracy in the energy and flux reconstruction throughout the use of one or more atmospheric instruments. Secondly, a precise and continuous monitoring of the atmosphere will allow for an increase of the telescope duty cycle with the extension of the observation time during hazy atmospheric conditions, which are normally discarded in the current experiments because of the uncertainty in the data reconstruction. Finally, a possible "smart scheduling", i.e., an adaptation – if required – of the observation strategy during the night that considers the actual atmospheric condition can be activated with a precise monitoring program of the atmospheric conditions.

In this document, we mainly focus on the importance of the use of Raman LIDARs to retrieve the differential atmospheric absorption at different wavelengths at the observatory site. We will show why the Raman LIDAR is expected to be an optimal instruments for CTA. There are currently three groups developing independently Raman LIDARs for CTA, but the interest around these instruments is increasing and possibly other groups will try to develop different solutions. In this document, we present the main design ideas behind these LIDARs and the progress in their construction.

2 Why CTA needs Raman LIDARs

LIDAR is an acronym for LIght Detection And Ranging. The methodology of the LIDAR technique requires the

---

1. www.mpi-hd.mpg.de/hfm/HESS/,
   wwwmagic.mppmu.mpg.de,
   veritas.sao.arizona.edu
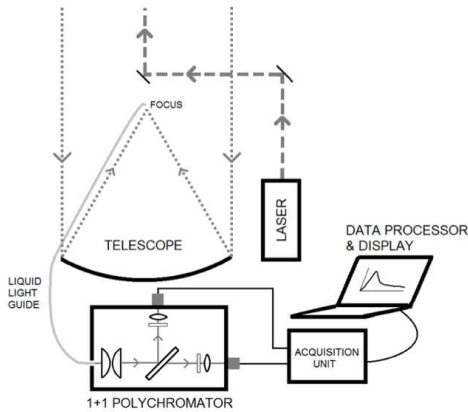
Figure 1: Schematic view of a possible Raman LIDAR for the CTA. A laser is pointed towards the atmosphere, and the backscattered light collected by a telescope. At the focal plane, a light guide transports the light to a polychromator unit which is controlled and readout by an acquisition system and a data processor unit.

transmission of a laser-generated light-pulse into the atmosphere (see Fig. 1). The amount of laser-light backscattered into the field of view of an optical receiver on the ground, is then recorded and analyzed. LIDARs have proven to be a powerful tool for environmental studies. Successful characterization of the atmosphere has been made at night using these systems [11, 12, 13], and in other fields of astronomy, the LIDAR technique has proven to be useful for the determination of the atmospheric extinction of starlight [14]. Of the various kinds of LIDARs, the so-called elastic one make only use of the elastically backscattered light from atmospheric molecules and particles, while the Raman LIDARs make also use of the backscattered light from roto-vibrational excitation of the sole atmospheric molecules and not the aerosols. Elastic LIDARs are the simplest class of LIDAR, but their backscatter power return depends on two unknown physical quantities (the total optical extinction and backscatter coefficients) which need to be inferred from a single measurement. As a result various assumptions need to be made, or boundary calibrations introduced, limiting the precision of the height-dependent atmospheric extinction to always worse than 20%. The introduction of additional elastic channels and/or Raman (inelastic-scattering) channels allows for simultaneous and independent measurement of the extinction and backscatter coefficients with no need for *a priori* assumptions [12]. Raman LIDARs yield a precision of the atmospheric extinction at the 5% level.

The LIDAR return signal can be described by the LIDAR equation:

$$P(R, \lambda_{rec}) = K \frac{G(R)}{R^2} \beta(R, \lambda_{em}) T^{\uparrow}(R, \lambda_{em}) T^{\downarrow}(R, \lambda_{rec}) \quad , \tag{1}$$

which contains a system factor K (emitted power, pulse duration, collection area of the telescope), a geometrical overlap factor (overlap of the telescope field-of-view with the laser light cone) $G(R)$, the molecular and aerosol backscatter coefficient $\beta(R, \lambda_{em})$ and the transmission terms $T^{\uparrow}(R, \lambda_{em})$ and $T^{\downarrow}(R, \lambda_{rec})$. R is the atmospheric range, i.e. the distance from the LIDAR optical receiver, and $\lambda_{em,rec}$ are the emitted and received wavelengths.

Using the elastic and Raman-scattered profiles, the atmospheric aerosol extinction coefficients $\alpha^{m,p}$ (m stands for molecules and p stands for particles or aerosol) can be derived with good precision. In this case, the inversion equation has only the so-called Ångström index as free parameter (if only one elastic-Raman wavelength pair is used) and over- or underestimating the Ångström index by 0.5 leads to only 5% relative error in the extinction factor. Hence, apart from statistical uncertainties (which can be minimized by averaging many LIDAR return signals), results are typically precise to about 5-10% **in each altitude bin**, and probably even better in clear free tropospheres with only one aerosol layer. The uncertainty generally grows with increasing optical depth of the layer. By adding a **second Raman line**, e.g. the N_2 line at 607 nm, the last free Ångström parameter becomes fixed, and precision of **better than 5%** can be achieved for the aerosol extinction coefficients. The molecular extinction part needs to be plugged in by hand using a convenient model. However, since the molecular densities change very little, and on large time scales, this can be achieved by standard tools. Precision of typically better than 2% are rather easy to achieve.
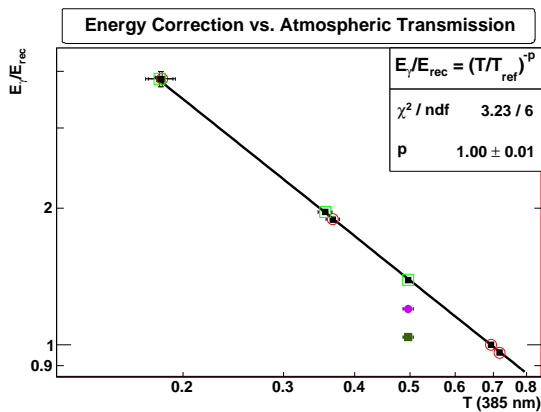
Although IACTs are normally placed at astronomical sites, characterized by extremely good atmospheric conditions, the local atmosphere is potentially influenced by phenomena occurring at tens to thousands of kilometers away, and thus should be continuously monitored. While the molecular content of the atmosphere varies very slowly at a given location during the year, and slowly from place to place, aerosol concentrations can vary on time-scales of minutes and travel large, inter-continental, distances. Most of them are concentrated within the first 3 km of the troposphere, with the free troposphere above being orders of magnitude cleaner. Aerosol sizes reach from molecular dimensions to millimeters, and the particles remain in the troposphere from 10 days to 3 weeks. The sizes are strongly dependent on relative humidity. Different types of aerosol show characteristic size distributions, and an astronomical site will always show a mixture of types, with one possibly dominant type at a given time and/or altitude. Light scattering and absorption by aerosols needs to be described by Mie theory or further developments of it, including non-sphericity of the scatterer. Aerosols generally have larger refraction indexes than that of water, and typically show also a small imaginary part. Contrary to the typical λ^{-4} wavelength dependency of Rayleigh-scattering molecules, aerosols show power-law indexes (the so-called *Ångström* coefficients) from 0 to 1.5, i.e. a much weaker dependency on wavelength.

In order to estimate the effect of different atmospheric conditions on the image analysis of IACTs, we have simulated different molecular and aerosol profiles for the MAGIC system, consisting of two telescopes. The results were presented in a master thesis and elsewhere in this conference [8, 7]. Several aerosol scenarios were simulated: *i*) enhancements of the ground layer from a quasi aerosol-free case up to a thick layer which reduces optical transmission by 70%, *ii*) a cloud layer at the altitudes of 6 km, 10 km (cirrus) and 14 km (volcano debris) a.s.l., and *iii*) a 6 km cloud layer with varying aerosol densities. The main results can be summarized in three points:

1. Using correct MC, energy and flux reconstruction is correct, at only the expense of a larger energy thresh-

old, which can be explained by the fact that with hazy atmospheres fewer photons reach the ground;

2. In the case that the aerosol overdensity or cloud is below the electromagnetic shower, a simple correction method can be used to restore correct energy and flux reconstruction with the simple use of standard Monte Carlo;

3. When the clouds or aerosol layer is at the shower development region or above, **the total extinction is no longer an useful parameter**

Energy Correction vs. Atmospheric Transmission

$$E_\gamma/E_{rec} = (T/T_{ref})^{-p}$$

χ^2 / ndf   3.23 / 6

p 1.00 ± 0.01

Figure 2: Energy reconstruction as a function of the total transmission at 385 nm. The linear dependence is valid only in the case of low aerosol overdensities. E_{rec} is the reconstructed energy from an initial Monte Carlo event with energy E_γ. T_{ref} is a scale transmission at 385 nm and $-p$ the chi-square optimized index, T is the transmission at 385 nm for each of the points in the plot. See text for additional details. Taken from [7].

The last two points are shown in Fig. 2 where the energy correction is shown as a function of the total transmittance at 385 nm. One can see that in the case that the aerosol overdensity is located close to the ground, i.e. below the electromagnetic shower development, then the energy reconstruction is precisely obtained from the total transmission, while if the overdensity is above, then correlation is broken and **height-resolving instruments are required**. This is the main motivation for the need of a Raman LIDAR instrument for CTA. We believe that the main findings of this study should also be valid for CTA, at least in the energy range from 50 GeV to 50 TeV. Previous studies have been made [9, 4, 5] for H.E.S.S. and for the MAGIC mono system, however only for an increase of low-altitude aerosol densities, and in [10] for a reference configuration of CTA, claiming a change in the spectral power-law index of gamma-ray fluxes, when atmospheric aerosol layers are present. In our work, we found that different atmospheres affect the energy threshold, the energy resolution and the energy bias, that propagate into the computation of a target flux and spectral reconstruction. See [8, 7] for further details.

Atmospheric properties can be derived, to a certain extent, also directly from IACT data. Several studies have been made by the H.E.S.S. and MAGIC collaborations to estimate the integral atmospheric transmission, using trigger rates, muon rates, combinations of both [6], or the anode currents of the photomultipliers and/or pedestal RMS.

Up to now, these parameters have been used only to discard data taken under non-optimal conditions, but work is ongoing to use this information to also correct data. However, as stated above, the use of integral transmission parameters is only valid in some of the possible atmospheric scenarios. In addition, data obtained directly from the telescopes suffer from the fact that instrumental properties (e.g. mirror reflectivity, PMT aging, etc) could influence these data, and therefore the separation between purely atmospheric effects could be affected. Anyhow, we have investigated the possibilities of using remote sensing devices such as the LIDAR. The experience of MAGIC with an elastic LIDAR system (i.e. analyzing only one backscatter wavelength, and no Raman lines), has shown that simplified reconstruction algorithms can be used to achieve good precision of the aerosol extinction coefficients, at least within the range of uncertainties inherent to an elastic LIDAR [15]. An analog conclusion was achieved with the H.E.S.S. LIDAR: a stable analysis algorithm was found, limited by the 30% uncertainties of the time and range dependent LIDAR ratio.

3 Raman LIDARs prototypes

Several institutes in CTA are currently designing Raman LIDAR systems: the Institut de Fìsica d'Altes Energies (IFAE) and the Universitat Autònoma de Barcelona (UAB), located in Barcelona (Spain), the LUPM (Laboratoire Univers et Particules de Montpellier) in Montpellier (France) and the CEILAP (Centro de Investigaciones Laser y sus Aplicaciones) group in Villa Martelli (Argentina). The different groups are designing independently the LIDAR systems with different mechanical, optical and steering solutions. In addition, two other groups have shown interest in discussing new designs for Raman LIDARs, one in Adelaide (Australia) and one from INFN (Italy). We anticipate that these designs are not necessarily in competition, and that the fact that CTA will have two different sites, one in the Northern and one in the Southern hemisphere, and that CTA could be operated also with different sub-arrays pointing at different directions in the sky, could possibly require the use of several Raman LIDARs at the same site. However, the overall strategy is not defined yet. Some information about the different LIDAR is collected in Table 1.

3.1 CEILAP design
Contact: P.Ristori (pablo.ristori@gmail.com)
The CEILAP group is developing a fully custom-made multi-wavelength scanning Raman LIDAR in the frame of the Argentinean CTA collaboration. This LIDAR emits laser pulses of $7-9$ ns duration at 355, 532 and 1064 nm and at 50 Hz with nominal energy of 125 mJ at 1064 nm and records these wavelengths and the two nitrogen Raman shifted wavelengths from 532 nm (607 nm) and 355 nm (387 nm). A sixth wavelength at 408 nm is also used to detect the water vapor Raman return. The system is peculiar because it uses six commercial 40 cm diameter parabolic mirrors with $f/2.5$ that can be used as six independent Newtonian telescopes. This permits to avoid dealing with typical deformation, aberration issues and higher costs that are usually connected with larger mirrors. This solution also permits to possibly extract any mirror for recoating or exchanged keeping the other five mirrors operating. Furthermore mirror construction and coating can be done by standard methods. The main drawback of the chosen so-

	CEILAP	IFAE/UAB	LUPM
Housing	Custom-made container	CLUE container	CLUE container
Design	Multi-angle	Co-axial	Co-axial
Mirror diameter [cm]	6x40	1x180	1x180
Mirror f/D	2.5	1	1
Elastic 355 nm	X	X	X
Raman 387 nm (N_2)	X	X	X
Raman 408 nm (H_2O)	X		
Elastic 532 nm	X	X	X
Raman 607 nm (N_2)	X	X	X
Elastic 1064 nm	X		
Laser	Continuum Inlite-II	Quantel Brilliant	Quantel CFR400
Max. Laser power [mJ/p]	125 @ 1064 nm	100 @ 355, 532 nm	90
Pulse duration [ns]	$7-9$	5	7
Beam diameter [mm]	6	6	7
Beam divergence [mrad]	< 0.75	0.5	3.5
Pulse frequency [Hz]	50	20	20
Light transport	Optical fiber	Liquid lightguide	Liquid lightguide
	Edmund UV/VIS series	Lumatec Series 300	Spectral Labs.
Fiber size [mm]	1	8	8
Fiber N.A. [mm]	0.22	0.64	0.6
Photon detector	PMT	PMT/HPD	PMT
	Hamamatsu H10721-110*	Hamamatsu R11920-100*	Hamamatsu R329P
Cathode diameter [inch]	1	1.5	2
Readout system	LICEL	LICEL	LICEL

Table 1: Data collection of the Raman LIDARs for CTA. *Subject to change.
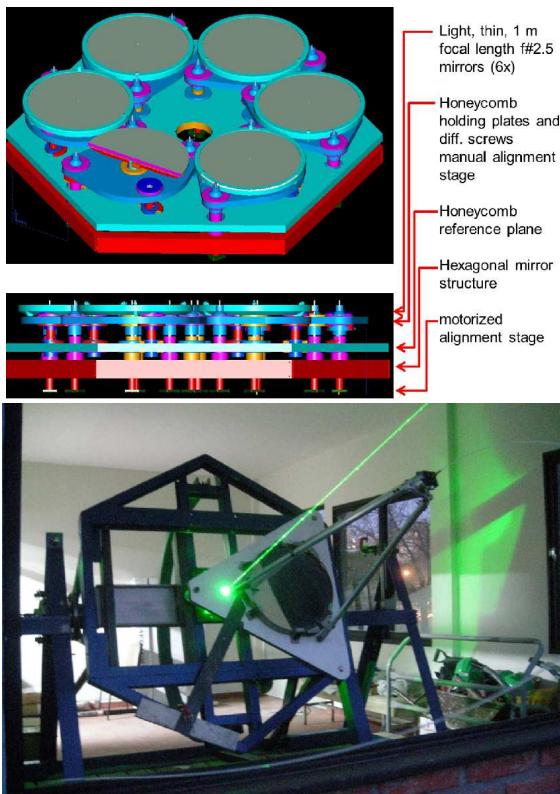
Figure 3: (top) Multi-mirror setup of the LIDAR system from the top and lateral view showing the different stages of the system. (bottom) The first sector of the LIDAR mounted and tested.

lution is that each of the six telescopes must be aligned properly to attain the maximum system efficiency. The additional alignment procedure has been solved by an automatic mirror alignment to follow the line of sight of the observation during the acquisition period. For this, each mirror is equipped with actuators on their backsides. The system was designed to operate in hard environmental conditions. A image of the LIDAR is shown in Fig. 3.

The multi-mirror telescope unit was designed to provide a maximum stability to the system with a minimum weight. While honeycomb was used for the multi-mirror reference plane, carbon fiber tubes were used to place the optical fiber at the mirror focal plane. Nylon pieces were synterized at the end of the carbon tubes to provide better fixation. The laser model is Inlite II-50 from Continuum. It has a hardened design and compact size for reliable operation in industrial environments. The flash-lamp can be easily removed for future maintenance. It has a cast aluminum resonator structure which ensures long-term thermal and mechanical stability. The optical fibers are standard 1 mm size. The optical module unit is totally custom-designed and custom-made, with the main structure being built with 3d printing machines. For the PMTs, bialkali (UBA) or superbialkali (SBA) modules from Hamamatsu are foreseen. Possible choices will be H10721-220 (UBA) o H10721-110 (SBA). During 2012 a new shelter-dome to host the LIDAR was acquired. A standard 20 ft container was cut and equipped with hydraulic pistons. The whole LIDAR is remotely controlled using a wi-fi link from the control PC to the LIDAR shelter creating a local LIDAR network under the TCP/IP protocol. Both acquisition and shelter controls will be operated remotely by the shifter. This control system is fully functional. The operation scheme is presented in [23].

The first sector of the LIDAR is currently mounted and under tests together with the laser and the alignment system. The final telescope steering system is under development as well as the motorized azimuth-zenithal mechanism in acquisition process [23]. The next steps are designing the spectrometric box and building the electronic control in its final version. For the optical module, photomultipliers from Hamamatsu H10721-110 are foreseen for all channels.

3.2 IFAE/UAB design
Contact: M.Gaug (markus.gaug@uab.cat)
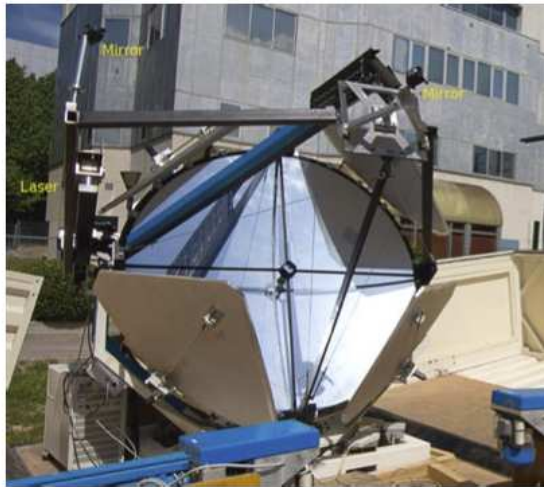
Figure 4: The Barcelona IFAE/UAB Raman LIDAR. A similar LIDAR is being assembled by LUPM.

Fig. 4 shows an image of the Barcelona Raman LIDAR. The telescope structure and housing container has been inherited from the former CLUE experiment and is currently being refurbished for its adaptation to a LIDAR system [17]. It is composed of a steel structure, over which a primary mirror is fixed. The mirror is a solid glass parabolic dish of 1.8 m diameter with an $f/1$ and thickness of 6 mm obtained with hot slumping technique developed at CERN. The point spread function of the mirror is about 6 mm while its reflectivity has degraded compared to the CLUE times and is currently about 60%. For this reason the mirror will be refurbished in the future. The telescope was equipped with a Nd:YAG laser from Quantel Brilliant emitting at the primary wavelength of 1064 nm with the first two harmonics available at 532 and 355 nm. The energy per pulse is 60 mJ, the pulse repetition frequency is 20 Hz and the pulse duration 5 ns, with a beam waist of 6 mm and divergence of 0.5 mrad. The laser is mounted at the side of the telescope, as shown in Fig. 4 and two small guiding mirrors mounted in front of the laser, guide the laser light to the optical axis of the telescope. The LIDAR is therefore called mono-axial. At the focal plane, a liquid light-guide from Lumatec Series 300 collects the light of the mirror. It has an 8 mm diameter section, a numerical aperture of 0.59 and transitivity of more than 0.7 in UVs for the whole length. The guide was tested and its performance are quite stable over the working temperature range. The main problem is that it cannot transport the 1064 nm line from the laser, which needs to be masked. In addition, the numerical aperture is relatively large due to the large size of the fiber. The liquid light-guide transports the light to an optical unit called a polychromator which collimates the beam and transports the light to four photomultipliers for the four wavelengths of interest (the two elastic at 355 and 532 nm and two N2 Raman lines at 387 and 607 nm) [22]. The polychromator will be mounted in the back of the telescope structure and will move together with the telescope. The current baseline design foresees PMTs from Hamamatsu. We will use for some channels Hamamatsu R11920-100 of 1.5 inch size (those used for CTA LST cameras), and possibly Hamamatsu H10425-01 for the 607 nm line, because it has a larger efficiency. However, the possible use of custom Hybrid Photon Detectors (HPD) is still under consideration. The needed cathode size either for PMT or HPD is at least 20 mm diameter. Dichroic mirrors and collimating lenses are already acquired and the assembly is currently under tests now. The acquisition unit is based on commercial LICEL^{TM} modules. The telescope steering is tested and fully functional. The next step is the assembly of the polychromator unit and the test of the full LIDAR system. Primary tests will be done in Barcelona and fields test will be done in La Palma at the MAGIC telescope site.

3.3 LUPM design
Contact: G. Vasileiadis (george.vasileiadis@lpta.in2p3.fr)

The LUPM design is similar to that of the IFAE/UAB Raman LIDAR. It is also based on the use of the CLUE container and telescope structure. However, different solutions for the laser, the telescope and container steering, readout wavelengths, etc. were chosen. In particular, due to age and relatively difficulty to obtain parts, LUPM opted for a completely rebuilt of all mechanical parts of the container. New motors were purchased and installed both for the container doors operations and the telescope movement. A completely new automated system, based on the Rockwell automation PowerFlex series, will take care of the drivers guidance and mechanical operation of the LIDAR. A dedicated Ethernet based software environment will assure the user operation. The communication with the rest of the CTA DAQ system will be done over the OPC/UA protocol.

Due to the harsh conditions expected for the southern hemisphere CTA observatory where some of the LIDARs will be installed, LUPM opted for an industrial/military-type of laser. Their choice was a CFR400 laser fabricated by Quantel. The CFR laser is a lamp pumped Nd:YAG laser featuring a degree of ruggedization not found in typical scientific lasers. The CFR design has been vibration-tested and each laser is temperature cycled before shipping. It emits at 1064,532 and 355nm with a peak energy of 90 mJ and 20 Hz repetition rate. It has a 7 ns pulse duration, beam diameter less than 7 mm and beam divergence better than 3.5 mrad. The laser will be mounted in one of the telescope masts, while a beam drive system will assure a coaxial operation of the LIDAR. Collection at the focal point of the telescope will be achieved using a liquid fiber, Spectra Labs, of 8 mm diameter, 5 m long and numerical aperture of 0.6 with a transmissivity of more than 0.6 in the UV. A traditional optical box where the necessary Raman filters and beam splitters and attenuators will be mounted at the back of the telescope. In total we will detect four wavelengths, with the same specs as of the IFAE/UAB design. A set of Hamamatsu photomultipliers tubes of 2 inches diameter will detect the incoming signal, while data acquisition will be assured by a LICEL commercial system.

3.4 Other possible contributions
The atmospheric calibration is raising larger interest in the CTA community and two additional groups are currently evaluating the possibility to contribute with independent designs of Raman LIDARs. The first group relates to the University of Adelaide [21] (contact: I. Reid and A. MacKinnon), whose current work is based on monitoring of greenhouse gases and climate change. The Atmospheric Physics Group in collaboration with the Optics and Photonics Group is setting up a new LIDAR facility at Buck-

land Park. The aim is to measure atmospheric temperature, wind and dynamical processes with high spatial and temporal resolution from 10 to 110 km altitude. It is possible that they can use the facility to build a Raman LIDAR for the needs of CTA. A second group is formed by the INFN (Italian Institute for Nuclear Physics) sections of Napoli, Padova and Torino (contact: C. Aramo (aramo@na.infn.it)), with a long-standing experience with the Raman LIDAR and the atmospheric calibration for the Auger experiments. The groups are joining interests for the construction of Raman LIDARs for CTA.

4   Complementary instrumentation

Apart from the Raman LIDAR, complementary devices for atmospheric characterization and the understanding of the site climatology can be used. A first class of devices comprises those which provide at least some profiling of the atmosphere, such as radio sondes, profiling microwave or infrared radiometers and differential optical absorption spectrometers. The operating wavelengths of these devices are very different from those of the Raman LIDAR, and precise conversion of their results to the spectral sensitivity window of the CTA is difficult. However, since aerosols are better visible at larger wavelengths, profiling devices may be used to determine cloud heights with high precision and their results may be good seeds for the Raman LIDAR data inversion algorithm. A next class of complementary devices contains those which measure integral parameters, such as Sun, Lunar and stellar photometers, UV-scopes and starguiders. Integral optical depth measurements have become world-wide standards, organized in networks ensuring proper (cross-)calibration of all devices. Spectacular resolutions of better than 1% can be obtained during the day, about 2% with moon, and 3% under dark night conditions, at wavelength ranges starting from about 400 nm. Extrapolations to the wavelength range between 300 and 400 nm worsens the resolution again. The precise results from these devices can serve as important cross-checks of the integrated differential Raman LIDAR transmission tables. Finally, all major astronomical observatories operate cloud detection devices, mainly all-sky cameras and/or take advantage from national weather radars. All-sky cameras have become standardized within the CONCAM or the TASCA networks, however important differences in sensitivity to cirrus clouds are reported. The advantage of these devices are their big field-of-view which allows to localize clouds over the entire sky and makes possible online adapted scheduling of source observations. Relatively cheap cloud sensors based on pyrometers or thermopiles have been tested by the MAGIC collaboration and the SITE WP of CTA. The calibration of these devices is however complex and measurements are easily disturbed by surrounding installations. Recent analysis can be found in [18, 19].

5   Conclusions and outlook

Monte Carlo simulations showed that while data affected by enhancements of the ground layer can be scaled rather easily up to high levels of extinction, this is not the case anymore for (cirrus) clouds at altitudes from 6 to 12 km a.s.l., which create strong energy-dependent effects on the scaling factors. Moreover, the images from atmospheric showers are distorted depending on the location of the shower maximum, which varies even for showers of a same

energy. Very high altitude layers, in turn, produce only effects on the very low energy gamma-ray showers. Depending on the properties of the chosen site for CTA, still to be decided, it would probably make sense to create $10-20$ typical atmospheric simulations within these possibilities and interpolate between them. The natural solution is the use of (Raman) LIDARs, which were described in this contribution. However, the use of complementary instruments that measure integral or differential (in altitude) atmospheric parameters is possible and envisaged. Once retrieved the differential atmospheric transparency, different strategies may be foreseen to accurately and precisely reconstruct data, ultimately reducing the reconstructed energy and flux uncertainties. This can be achieved by re-calibrating the data themselves, either event-wise or bin-wise, or by simulating adapted atmospheres [20]. In addition, it would be possible to increase the duty cycle of the telescopes by retrieving those data taken during non-optimal atmospheric conditions which are normally discarded by standard clean-atmosphere analysis, especially important during e.g. multi-wavelength campaigns or target of opportunity observations.

Three independent groups are currently developing custom-made Raman LIDARs. In Argentina, CEILAP is developing a novel-design 6-mirror Raman LIDAR, while in Europe, IFAE/UAB in Spain and LUPM in France are adapting a telescope from the terminated CLUE experiment as Raman LIDAR. Status and plans were reported in this proceedings.

References

[1] M. Actis et al., Exper.Astron. 32 (2011) 193-316.

[2] J. Aleksić et al., Astrop.Phys. 35 (2012) 435-448

[3] F. Aharonian et al., A&A 457 (2006) 899-915

[4] S. J.Nolan et al., Procs. 30th ICRC (2007)

[5] D. Dorner et al. A&A 493 (2009) 721-725

[6] R. De Los Reyes et al, Procs. 33rd ICRC (2013) ID-0610

[7] D. Garrido et al., these proceedings.

[8] D. Garrido. Phd Thesis. Univeristat Autónoma Barcelona (2011)

[9] K. Bernlöhr, Astrop.Phys. 12 (2000) 255-268

[10] S.J. Nolan et al., Astrop.Phys. 34 (2010) 304-313

[11] H. Inaba, Springer-Verlag, New York (1976) 143

[12] A. Ansmann et al., Appl.Opt. 31 (1992) 7113

[13] A. Behrendt et al., Appl.Opt. 41 (2002) 7657

[14] P.C. Zimmer et al., Procs. AAS Meeting, 42 (2010) 401

[15] C. Fruck et al., Procs. 33rd ICRC (2013) ID-1054.

[16] P. Ristori et al., Procs. 33rd ICRC (2013) ID-0346.

[17] A. Lopez-Oramas et al., Procs. 33rd ICRC (2013) ID-0210.

[18] M. Daniel and G. Vasileiadis, AIP Conf. Procs. 1505 (2012) 717-720

[19] J. Hahn et al., AIP Conf. Procs 1505 (2012) 721-724

[20] M. Doro *et al.* [CTA Coll.], Procs. 33rd ICRC (2013) ID-0151

[21] http://www.physics.adelaide.edu.au/atmospheric/lidar.html

[22] V. Da Deppo et al., Proc. of SPIE Vol. 8550 85501V-1.

[23] J. Pallotta et al., Procs. of the AtmoHEAD Conf., Saclay (2013)